Geophys. Res. Lett. Published on March 31, 2007

Slow Postseismic Recovery of Geoid Depression Formed by the 2004 Sumatra-Andaman Earthquake by Mantle Water Diffusion

Ryoko Ogawa,[1] and Kosuke Heki [2]

[1]Div. Earth Planet. Sci., Graduate School of Science, Hokkaido University, N10 W8, Kita-ku, Sapporo-city, 060-0810, Japan
[2]Dept Natural History Sci., Faculty of Science, Hokkaido University, N10 W8, Kita-ku, Sapporo-city, 060-0810, Japan

Abstract

Earthquakes are accompanied with mass redistributions and cause changes in gravity field and shape of geoid, an equipotential surface coincident with the mean sea surface. Such coseismic changes were detected by satellite gravimetry after the 2004 Sumatra-Andaman Earthquake [*Han et al.,* 2006], but little has been known on what happens on geoid after the earthquake. Here we report slow postseismic recovery of coseismic geoid depression from satellite measurements. This cannot be explained with simple afterslip or viscous relaxation of Maxwellian upper mantle. It suggests the relaxation of coseismic dilatation and compression by the diffusion of supercritical H_2O abundant in the upper mantle. Such a self-healing system of coseismic geoid undulations, a brand-new role of water in mantle, would significantly reduce the amount of permanent shifts of the Earth's rotation axis by earthquakes.

1. Introduction

The Earth's monthly gravity fields recovered by GRACE (Gravity Recovery and Climate Experiment) satellite, launched in 2002, have been improving our knowledge on time-variable mass distributions on the Earth including lithospheric rebound by on-going ice melting [*Tamisiea et al.,* 2005], seasonal hydrological cycles in river basins [*Tapley et al.,* 2004], water loss by drought in tropical regions [*Crowley et al*., 2006], and seasonally changing mass in semi-closed ocean basins [*Fenoglio-Marc et al*., 2006]. The great Sumatra-Andaman Earthquake, 2004 December 26, ruptured the eastern boundary of the Indian Plate extending >1000 km from Sumatra to the Andaman Islands causing devastating tsunami in the Indian Ocean [*Ammon et al*., 2005]. This earthquake has been studied with various approaches such as tsunami observations with tide gauges [*Tanioka et al.,* 2006] and satellite altimetry [*Hirata et al.*, 2006], crustal movement with Global Positioning System (GPS) [*Vigny et al.*, 2005], and ionospheric disturbances [*Heki et al.,* 2006]. This was also the first earthquake whose coseismic gravity changes have been detected by the GRACE satellite measurements [*Han et al.,* 2006].

2. Co- and postseismic changes in geoid

2-1. Calculation of coseismic changes in geoid height

Earthquakes modify geoid height by two kinds of mass distribution perturbations, (1) deformation of layer boundaries with density contrasts, and (2) the density changes of rocks. Uplift and subsidence of the ocean floor and Moho cause (1) and coseismic dilatation and compression of crustal and mantle rocks cause (2). Here we calculate such coseismic geoid height changes a little differently from *Han et al.* [2006]. First we assume fault parameters by *Banerjee et al*. [2005] and calculate surface and Moho

uplift/subsidence and volume strain in an elastic homogeneous half space [*Okada*, 1992]. Difference from a more realistic approach assuming spherical and layered Earth would be <10 % because mass perturbations contributing to geoid deformation mostly occur within 100 km from the fault [*Cummins et al*., 1998]. Secondly, we calculated geoid height changes by integrating scalar potentials at the geoid surface from these perturbing masses (= Gdm/r, where dm is the small perturbing mass at distance r from the point on geoid, and G is the universal gravity constant) and by dividing them with gravitational acceleration. Following *Han et al.* [2006], ocean floor was assumed 3 km below geoid and Moho 20 km further below, and the distance r was calculated assuming spherical Earth. We used the same mantle, crust, and seawater densities as *Han et al.* [2006].

Fig.1 shows the calculated coseismic geoid height changes and their east-west profile. The uplift/subsidence signature is confined near the fault, while dilatation/compression signature extends farther away. The total geoid change is downward throughout the region although a small ridge of geoid is formed along the arc (peak at ~93E). Spatial averaging, often performed to suppress noisy high degree/order components in GRACE data [*Wahr et al*., 1998], blurs such short wavelength components (see dashed curves in Fig. 1B). Therefore the coseismic geoid change observed with GRACE, using a realistic averaging radius, would look like a plain oval depression. Dominance of downward geoid changes is the manifestation of the essence of plate subduction, a downward movement of material. Such a change in mass distribution would cause coseismic shift of the Earth's principal axis of inertia (the North Pole moves toward the epicenter if earthquakes occur in the northern hemisphere) [*Gross and Chao*, 2006], and contributes to the excitation of the Chandler wobble.

2-2. Observations with GRACE

By combining the Stokes' coefficients in the GRACE level 2 data [*Bettadpur*, 2003], monthly geoid height at a desired point is calculated (equation 1 of *Wahr et al*. [1998]). We used such data (Release 1 from Center for Space Research, University of Texas) from 2002 April to 2006 October. Fig. 2 shows geoid height time series at points *a* and *b* (see Fig.1A, or Fig. 3A, B for positions). There we used the coefficients with degree/order complete to 80 and isotropic 350 km Gaussian filter to reduce short-wavelength noises [*Wahr et al*., 1998]. In addition to moderate amount of secular trend, the time series show strong seasonal (annual and biannual) signals that reflect yearly repeating hydrological and oceanographic cycles. To model these time series, we added two earthquake-related parameters, coseismic offset of the geoid height (unit: mm), and postseismic slow geoid height change proportional to a function, $1-e^{-t/\tau}$, where τ is a time constant and t is the time after the earthquake.

Fig. 2A shows a large coseismic downward jump of geoid consistent with Fig.1. Fig.2B shows a smaller coseismic jump, but its more notable feature is the significant coseismic change in trend and its decay. The trend change is positive (postseismic geoid upheaval), and the time constant τ as long as 0.6 year resulted in the best fit (Fig.2C, D). Fig. 3A, B shows, respectively, values of the coseismic geoid height changes and cumulative postseismic changes over the 1-year period, for 1° x 1° grid points. In order to stabilize the solution, the time constant of the decay of the postseismic changes τ is fixed to 0.6 year everywhere. Typical post-fit residuals of the geoid height time series were 1-2 mm. Geographic peaks of the coseismic and postseismic changes show some shift; the peak in coseismic geoid depression is located in the Andaman Sea while the postseismic geoid upheaval is the largest along the arc. In Fig. 3C, we compare profiles of the observed and the 350 km-filtered predicted geoid changes (filtering is done by disassembling predicted geoid height changes shown in Fig. 1A into Stokes' coefficients and by reassembling them after multiplying with the Gaussian filter in wave number domain [*Wahr et al*., 1998]). They are fairly consistent throughout the region, suggesting overall appropriateness of the above described procedures.

3. Model of postseismic geoid changes

3-1. Afterslip and viscous relaxation

The 1-year postseismic geoid uplift is statistically significant, and is comparable in amount to the coseismic subsidence (Fig. 3). This is the first detection of postseismic gravity/geoid changes with satellite gravimetry and its mechanism merits investigation. Interplate thrust earthquakes are usually followed by afterslips. They often release seismic moment comparable to main ruptures [*Heki et al.*, 1997]. Continuous GPS observations suggested that this earthquake is followed by an afterslip, with the moment not smaller than a few tens of percents of the main rupture [*Vigny et al.*, 2005; *Hashimoto et al.*, 2006]. Afterslips cause surface velocities similar in direction to coseismic jumps although actual directions are different in small scales owing to complementary distribution of co- and postseismic fault slips. They occur with time constants from days to years. The polarity reversal between co- and postseismic geoid changes found here suggests that simple afterslip model cannot explain the geoid behaviors in question.

Viscous relaxation of the mantle also causes slow surface displacements. For example, current oceanward crustal movements in Chile and western Argentine are explained by viscous flow of mantle rocks with Maxwell viscoelasticity (with the viscosity η of 2.5×10^{19} Pa s) induced by the 1960 Chilean Earthquake [*Hu et al.,* 2004]. Assuming similar viscosity structure in Sumatra, together with elastic modulus ε of 40 GPa, the Maxwell time η/ε becomes ~20 years, i.e. this mechanism would hardly explain the 0.6 year timescale changes discussed here. A Kelvin element viscosity, representing delayed elasticity in a biviscous rheology, of $\sim 5 \times 10^{17}$ Pa s is suggested to explain postseismic crustal deformation as beautifully as afterslip [*Pollitz et al*., 2006]. It is unclear, at the moment, if this successfully explains a part of the postseismic geoid recovery. In this study, we make a case for the third mechanism, water diffusion around the down-dip end of the fault.

3-2. Diffusion of water

Pore fluid diffusion causes postseismic changes opposite to coseismic ones with relatively short timescales [*Jónsson et al*., 2003]. Dilatation and compression associated with faulting disturb pore fluid pressure, and the fluid diffuses from the region with increased pressure (compression part) to the decreased region (dilatation part) [*Nur and Booker*, 1972]. This has been supposed to occur in the uppermost crust, but we here suggest that it may occur deep in the mantle by supercritical water that abundantly exists in subduction zones.

For a thrust earthquake, a pair of increased/decreased pore pressure changes is formed at the down-dip end of the fault (Fig.4A), where flow from the red to blue parts would occur following the pressure perturbation. Gravity would also encourage such upward flow in order to recover hydrostatic equilibrium disturbed by the density decrease of the shallow layer. Such mantle water flow will continue until the driving forces (pressure gradient and gravity) vanish under the new hydrostatic equilibrium. By then, the dilatation signal in geoid will be relaxed while dilatation/compression of the solid part (crustal and mantle rocks) remains almost intact. Two questions arise here, (1) if mantle water can diffuse that fast, and (2) if mantle water is ample enough to allow such an adjustment. As for (2), the coseismic volume strain is mostly within 10^{-5} level (Fig. 4A), and the weight percent of H_2O down there is much larger than this as discussed later. So movement of just a small portion of the total water could compensate density perturbation caused by such small dilatation/compression.

The question (1) needs some discussions. The pressure difference lets the pore pressure obey diffusion equation with the time constant τ of $L^2/4c$, where L is typical travel distance of fluid and c is the pore pressure diffusivity [*Nur and Booker*, 1972]. The diffusivity is given by $c = k/\eta\beta$, where k is permeability,

η is the viscosity of pore fluid, and β is bulk compressibility [*Nur and Booker*, 1972]. We inferred the permeability k after *McKenzie* [1984], in which k scales with ϕ^3 (ϕ is the volume percent of the pore fluid). Fig.4B shows τ as a function of ϕ, and for different values of L and η. The quantity β was fixed to 2.5×10^{-11} Pa^{-1}. Due to ambient high pressure and temperature, water (or H_2O) behaves as supercritical fluid whose viscosity is closer to gas (10^{-5} Pa s level) than to liquid (10^{-3} Pa s level). The time constant τ of 0.6 year is realized with the volume percent of H_2O of ~1 % and with the viscosity ~10^{-5} Pa s. Water in oceanic crust of subducting slabs is released at the depth of a few tens of kilometers (depending on thermal structure), which then diffuses into the wedge mantle and serpentinize mantle rocks [*Iwamori*, 1998]. Recent petrologic studies suggest water content as high as 0.5 weight percent or more in the upper mantle of back arc [*Kelly et al.,* 2006]. Mantle water diffusion can therefore take place on a <1 year timescale required to fit postseismic geoid changes with reasonable hydraulic parameters.

4. Discussion

Afterslip causes uplift/subsidence and dilatation/compression similar to the main rupture, and may leave geoid depression signature similar to Fig. 1A. However, such geoid depression might recover to some extent by simultaneous diffusion of mantle water as the afterslip slowly goes on. Therefore geoid signal of afterslip may look different, i.e. composed more of uplift/subsidence signature and less of dilatation/compression signature. Fig. 3D shows the "model" postseismic geoid uplift profile, calculated as the mixture of the decay of the coseismic dilatation signature (inverse of the blue dashed curve in Fig. 1B, shown here as a dark gray curve), and of afterslip without dilatation (same as the red dashed curve in Fig. 1B, shown here in light gray). The model assumes that an afterslip with the one-year cumulative moment release equal to one half of the main rupture has occurred, and that one half of the coseismic dilatation signature has disappeared. This model is not unique, e.g. we could consider less afterslip and more decay of the coseismic dilatation, and vice versa. The reality would lie somewhere, but current resolution of GRACE does not allow further discussion. We did not consider viscous mantle relaxation here, but its contribution to geoid changes should grow in time and merits long-term attention.

The mantle water flow causes, by poroelastic rebound, crustal deformation that partly cancels afterslip GPS signatures, and it may cause underestimate of seismic moment released by afterslip. It would also cause postseismic uplift of the Andaman and Nicobar Islands, which is opposite to what the viscoelastic model predicts [*Pollitz et al.*, 2006], but is consistent with postseismic GPS observations there [*Freymueller et al.,* 2006]. Proper treatment of the poroelastic rebound would thus lead to better assessments of afterslips and viscous relaxations. From global point of view, it would call for downward revision of coseismic shifts of the Earth's figure axis, whose estimate is based on the conventional view of mass redistribution in earthquakes [*Gross and Chao*, 2006]. Water plays numbers of important roles in subduction zones. It causes non-volcanic tremors in the down-dip end of seismogenic zones [*Obara*, 2003], and moves in the wedge mantle encouraging magma genesis by lowering the solidus temperature [*Iwamori*, 1998]. Satellite gravimetry may have revealed its brand-new role, postseismic healing of coseismic geoid undulations by its diffusive adjustment.

References

Ammon, C.J., C., Ji, , H.-K. Thio, D. Robinson, S. Ni, V. Hjorleifsdottir, H. Kanamori, T. Lay, S. Das, D. Helmberger, G. Ichinose, J. Polet, and D. Wald, Rupture process of the 2004 Sumatra-Andaman Earthquake, *Science, 308*, 1133-1139, 2005.

Banerjee P., F.F. Pollitz, and R. Bürgmann, The size and duration of the Sumatra-Andaman Earthquake from far-field static offsets, *Science, 308*, 1769-1772, 2005.

Bettadpur, S. Level-2 gravity field product user handbook, GRACE 327-734, CSR Publ. GR-03-01, 17 pp, Univ. Of Texas

at Austin, Austin, Texas , 2003.

Crowley, J.W., J.X. Mitrovica, R.C. Bailey, M.E. Tamisiea, and J.L. Davis, Land water storage within the Congo Basin inferred from GRACE satellite gravity data, *Geophys. Res. Lett., 33*, L19402, doi:10.1029/2006GL027070, 2006.

Cummins, P.R., S. Hirano, and Y. Kaneda, Refined coseismic displacement modeling for the 1994 Shikotan and Sanriku-oki earthquakes, *Geophys. Res. Lett., 25*, 3219-3222 , 1998.

Fenoglio-Marc, L., J. Kusche, and M. Becker, Mass variation in the Mediterranean Sea from GRACE and its validation by altimetry, steric and hydrologic fields, *Geophys. Res. Lett., 33*, L19606, doi:10.1029/2006GL026851, 2006.

Freymueller, J. T., C. Rajendran, K. Rajendran, and A. Rajamani, Near-field postseismic deformation measurements from the Andaman and Nicobar Islands, *EOS Trans. AGU* **87**(52), Fall Meet. Suppl., Abstract U44A-03, 2006.

Gross, R.S. and B.F. Chao, The rotational and gravitational signature of the December 26, 2004 Sumatran earthquake, *Surv. Geophys., 27*, 615-632, 2006.

Hashimoto, M., N. Choosakul, M. Hashizume, S. Takemoto, H. Takiguchi, Y. Fukuda, and K. Fujimori, Crustal deformations associated with the great Sumatra-Andaman earthquake deduced from continuous GPS observation, *Earth Planets Space, 58*, 127-139, 2006.

Han, S.-C., C.K. Shum, M. Bevis, C. Ji, and C.-Y. Kuo, Crustal dilatation observed by GRACE after the 2004 Sumatra-Andaman Earthquake, *Science, 313*, 658-662, 2006.

Heki, K., S. Miyazaki, and H. Tsuji, Silent fault slip following an interplate thrust earthquake in the Japan Trench, *Nature, 386*, 595-597, 1997.

Heki, K., Y. Otsuka, N. Choosakul, N. Hemmakorn, T. Komolmis, and T. Maruyama, Detection of ruptures of Andaman fault segments in the 2004 Great Sumatra Earthquake with coseismic ionospheric disturbances, *J. Geophys. Res., 111*, B09313, doi:10.1029/2005JB004202, 2006.

Hirata, K., K. Satake, Y. Tanioka, T. Kuragamo, Y. Hasegawa, Y. Hayashi, and N. Hamada, The 2004 Indian Ocean tsunami: Tsunami source model from satellite altimetry, *Earth Planets Space, 58*, 195-201, 2006.

Hu, Y., K. Wang, J. He, K. Klotz, and G. Khazaradze, Three-dimensional viscoelastic finite element model for postseismic deformation of the great 1960 Chile earthquake, *J. Geophys. Res., 109*, B12403, doi:10.1029/2004JB003163, 2004.

Iwamori, H. Transportation of H_2O and melting in subduction zones, *Earth Planet. Sci. Lett., 160*, 65-80, 1998.

Jónsson, S., P. Segall, R. Pedersen, and G. Björnsson, Post-earthquake ground movements correlated to pore-pressure transients, *Nature, 424*, 179-183, 2003.

Kelley, K.A., T. Plank, T.L. Grove, E.M. Stolper, S. Newman, and E. Hauri, Mantle melting as a function of water content beneath back-arc basins, *J. Geophys. Res., 111*, B09208, doi:10.1029/2005JB003732, 2006.

McKenzie, D. The generation and compaction of partially molten rock, *J. Petrol., 25*, 713-765, 1984.

Nur, A. and J.R. Booker, Aftershocks caused by pore fluid flow? *Science, 175*, 885-887, 1972.

Obara, K. Nonvolcanic deep tremor associated with subduction in southwest Japan, *Science, 296*, 1679-1681, 2003.

Okada, Y. Internal deformation due to shear and tensile faults in a half-space, *Bull. Seism. Soc. Am., 82*, 1018-1040, 1992.

Pollitz, F. F., R. Bürgmann, and P. Banerjee, Post-seismic relaxation following the great 2004 Sumatra-Andaman earthquake on a compressible self-gravitating Earth, *Geophys. J. Int., 167*, 397-420, 2006.

Tamisiea, M.E., E.W. Leuliette, E.W., J.L. Davis, and J.X. Mitrovica, Constraining hydrological and cryospheric mass flux in southeastern Alaska using space-based gravity measurements, *Geophys. Res. Lett., 32*, L20501, doi:10.1029/2005GL023961, 2005.

Tanioka, Y., Yudhicara, T. Kusunose, S. Kathiroli, Y. Nishimura, S. Iwasaki, and K. Satake, Rupture process of the 2004 great Sumatra-Andaman earthquake estimated from tsunami waveforms, *Earth Planets Space, 58*, 203-209, 2006.

Tapley, B.D., S. Bettadpur, J. Ries, P. Thompson, and M. Watkins, GRACE measurements of mass variability in the Earth system, *Science, 305*, 503-505, 2004.

Vigny, C., W.J.F. Simons, S. Abu, R. Bamphenyu, C. Satirapod, N. Choosakul, C. Subarya, A. Socquet, K. Omar, H.Z. Abidin, and B.A.C. Ambrosius, Insight into the 2004 Sumatra-Andaman earthquake from GPS measurements in southeast Asia, *Nature, 436*, 201-204, 2005.

Wahr, J., M. Molenaar, and F. Bryan, Time variability of the Earth's gravity field: Hydrological and oceanic effects and their possible detection using GRACE, *J. Geophys. Res., 103*, 30205-30229, 1998.

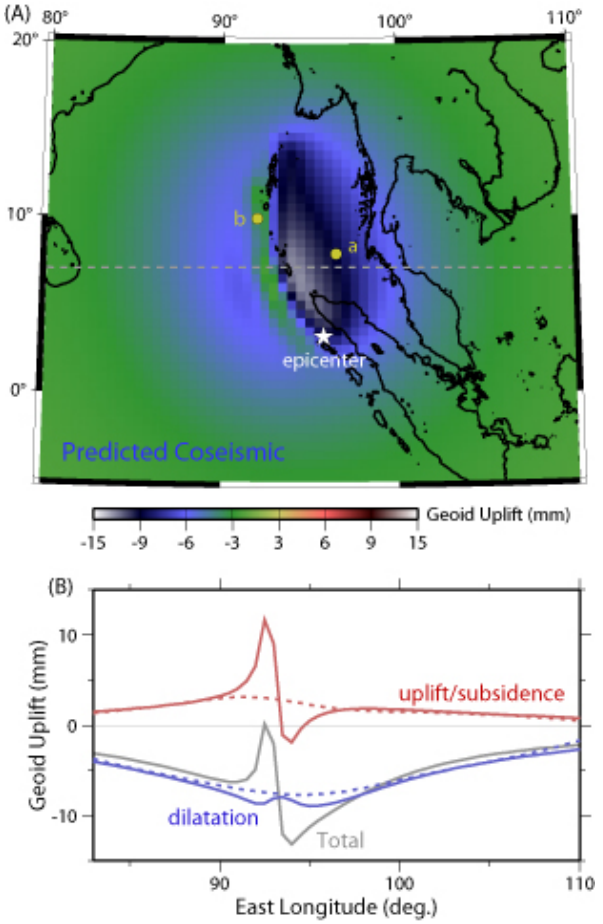

Fig.1. (A) Predicted coseismic change in geoid height and (B) its profile along the dashed line (N7.0) in (A). Contributions from uplift/subsidence of the ocean floor plus Moho, and those from dilatation plus compression of crust/mantle, and the total change, are shown by red, blue, and gray curves, respectively in (B) (dashed ones are those through the 350 km isotropic Gaussian filter [*Wahr et al.*, 1998]). Open star and yellow circles in (A) indicate, respectively, the epicenter and points where geoid height time series are shown in Fig. 2.

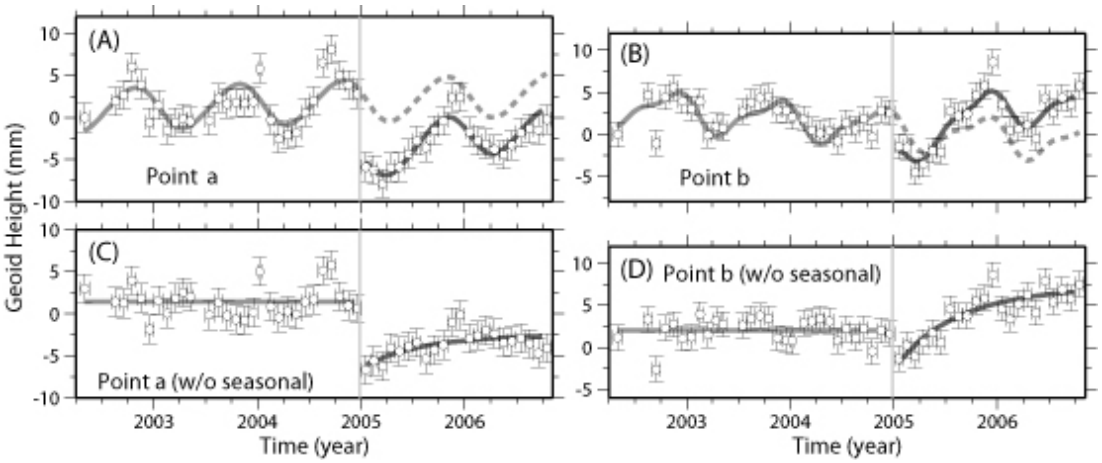

Fig.2. Time series of geoid height at the two points *a* (A) and *b* (B) (Fig.1A) calculated using GRACE level-2 data and 350 km isotropic Gaussian filter. Vertical gray lines show the occurrence time of the

2004 Sumatra-Andaman Earthquake. Light and dark gray curves indicate modeled time series before and after the earthquake (the former are extrapolated to the postseismic period as dashed curves to visualize their differences from the latter). Seasonal components are assumed same throughout the period. The error bars indicate time periods represented by individual data (horizontal bar) and a-posteriori 1σ measurement error to bring χ^2 unity after regression (vertical bar). The same time series are redrawn below (C and D) after removing secular and seasonal components.

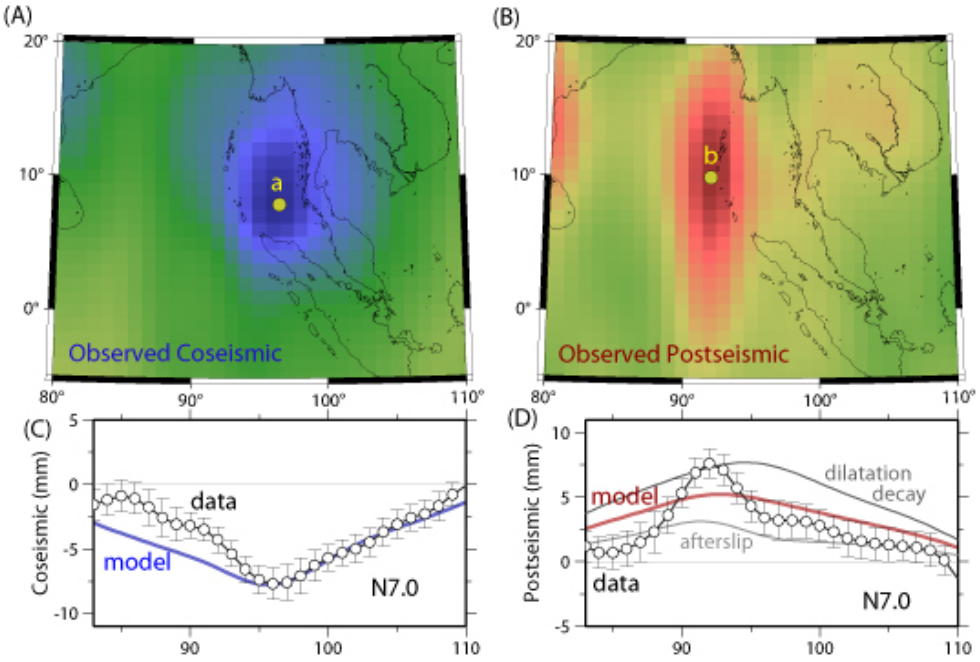

Fig.3. Geographic distribution of (A) coseismic jump of geoid height, and (B) 1-year cumulative postseismic geoid height change, are shown with the same color scheme as Fig. 1A. Their profiles along the dashed line in Fig.1A are shown in (C) and (D). 1σ error bars there are determined a-posteriori based on the post-fit residuals of the geoid height time series (Fig. 2). The model in (C) is obtained by performing 350 km isotropic Gaussian filter to the predicted total geoid changes in Fig. 1A. The two gray curves in (D) indicate possible contributions (also filtered) from the uplift/subsidence by the afterslip (with the 1-year cumulative moment as large as the main rupture), and from the total decay of coseismic dilatation. The model in (D) is obtained by combining the halves of the contributions from these two.

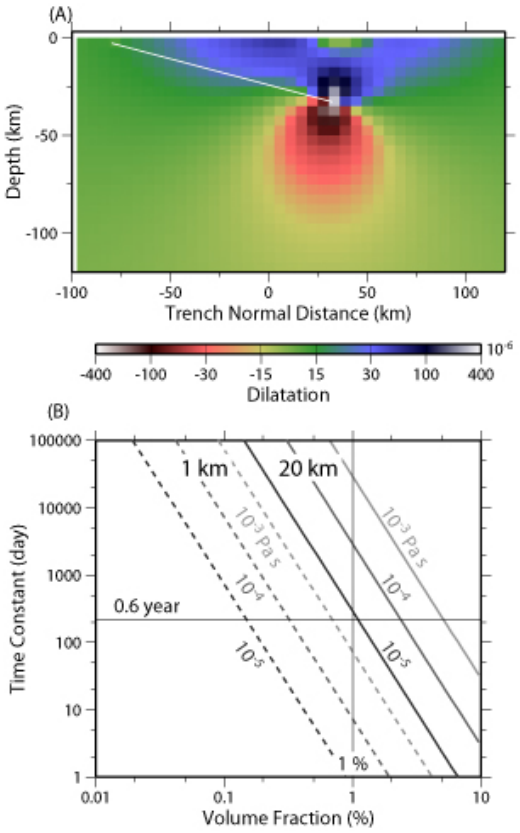

Fig.4. (A) Cross section of coseismic dilatation (blue) and compression (red) perpendicular to the fault strike at ~N7.0. The white line indicates the fault [*Banerjee et al.*, 2005]. (B) Time constant of the pore pressure diffusion for distances 1 km and 20 km as functions of the volume fraction of pore fluid. Three kinds of viscosity of the pore fluid, 10^{-3}, 10^{-4} and 10^{-5} Pa s, are assumed.